ACS APPLIED MATERIALS & INTERFACES

Research Article

www.acsami.org

(Pc)Eu(Pc)Eu[*trans*-T(COOCH$_3$)$_2$PP]/GO Hybrid Film-Based Nonenzymatic H_2O_2 Electrochemical Sensor with Excellent Performance

Zhenning Yu,[†] Lei Zou,[†] Yanli Chen,*[,†,‡] and Jianzhuang Jiang*[,‡,§]

[†]Shandong Provincial Key Laboratory of Fluorine Chemistry and Chemical Materials, School of Chemistry and Chemical Engineering, University of Jinan, Jinan 250022, China

[‡]School of Science, China University of Petroleum (East China), Qingdao 266580, China

[§]Beijing Key Laboratory for Science and Application of Functional Molecular and Crystalline Materials, Department of Chemistry, University of Science and Technology Beijing, Beijing 100083, China

Supporting Information

ABSTRACT: A facile approach was developed for preparing the multilayer hybrid films of mixed (phthalocyaninato) (porphyrinato) europium(III) triple-decker compound (Pc)Eu(Pc)Eu[*trans*-T(COOCH$_3$)$_2$PP] (**1**) and graphene oxide (GO) using the solution-processing QLS method. The combination of the nature of relatively high conductivity and great surface area for GO with the electroactive and semiconductive triple-decker compound in ITO electrode renders the hybrid film excellent sensing property for H_2O_2, due to the optimized triple-decker molecular packing in the uniform-sized nanoparticles (ca. 70 nm) formed on the GO surface. The amperometric responses are linearly proportional to the concentration of H_2O_2 in the range of 0.05−1800 μM with a fast response time of 0.03 s μM^{-1}, a low detection limit of 0.017 μM, and good sensitivity of 7.4 μA mM^{-1}. The present work represents the best result of tetrapyrrole-based nonenzymatic electrochemical sensor for H_2O_2. Nevertheless, the triple-decker/GO/ITO also shows excellent stability, reproducibility, and selectivity, indicating the great potential of electroactive tetrapyrrole rare earth sandwich compounds in combination with GO in the field of nonenzymatic electrochemical sensors.

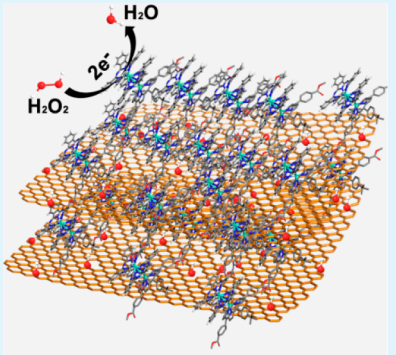

KEYWORDS: *graphene oxide, H_2O_2 sensor, hybrid film, phthalocyanine, porphyrin, rare earth*

INTRODUCTION

Detection of hydrogen peroxide (H_2O_2) has aroused a significant research interest for both academic purpose and practical applications in the fields of clinic, pharmaceutical, biosensing, and so forth.[1,2] Many analytical strategies including titrimetry,[3] spectrometry,[4] chromatography,[5] and fluorometry[6] have therefore been developed for the determination of H_2O_2 in the past decades. Practical applications of these methods however were retarded by their time-consuming and apparatus-specific nature. Therefore, much effort had been spent toward developing electrochemical method for detecting H_2O_2 that was simple, sensitive, and cost-effective.[7] Trials, however, revealed that either oxidation or reduction of H_2O_2 occurring at ordinary solid electrodes showed the slow electrode dynamics and large overpotential, which not only has a negative effect on the sensing performance but also results in great interference from other electroactive substances in practical electrochemical analysis for H_2O_2. Consequently, enzyme-involved biosensors were employed for the electrochemical analysis of H_2O_2. This method shows advantages of fast operation, good selectivity, and high sensitivity.[5,8,9] Unfortunately, the inherent instability of enzymes hinders their practical applications.[1] Developing nonenzymatic H_2O_2 electrochemical sensors with good stability and high performance is therefore of great importance.

Actually, as early as 1984, Prussian blue (PB) was employed as an electrochemical sensor for H_2O_2.[10] Despite the high catalytic activity of the PB-modified electrode, further investigation toward H_2O_2 electrochemical analysis was not continued due to its operational instability in the solution of pH ≥ 7 because Prussian white, the reduced form of PB, was gradually disintegrated by hydroxyl ions.[11] Thereafter, various materials such as noble metals, metal oxides, metallophthalocyanines, metalloporphyrins, redox polymers, and carbon nanotubes with enhanced electrochemical stability have been fabricated into corresponding electrodes for electrocatalytic H_2O_2 detection.[12] Due probably to the similar electrocatalytic active center employed by one well-known enzyme, heme protein, the tetrapyrrole (porphyrins/phthalocyanine)-modified electrodes toward the electrochemical analysis of H_2O_2 have been extensively studied.[13−19] Investigations revealed that both tetrapyrrole materials possessing improved electrocatalytic

Received: July 17, 2016
Accepted: October 19, 2016
Published: October 19, 2016

DOI: 10.1021/acsami.6b08760
ACS Appl. Mater. Interfaces XXXX, XXX, XXX−XXX

activity and controllable aggregation nature and electrodes with optimized charge migration between the electroactive centers of porphyrin/phthalocyanine and electrode are simultaneously necessary for the H_2O_2 electrochemical sensor with good performance.[2,9,20−23] Quite recently, a novel zinc porphyrin−fullerene derivative (ZnPor−C_{60}) was composed by covalently connecting ZnPor and C_{60} together and used to modify the electrode, resulting in the nice electrochemical sensing performance for H_2O_2 with the linear detection range of 0.035−3.40 mM, detection limit (LOD) of 0.81 μM, and sensitivity of 215.6 μA mM^{-1}.[24] In addition, the iron-tetrasulfophthalocyanine-graphene-Nafion nanocomposite film-based electrode was found to exhibit an extraordinary electrochemical sensing performance toward detection of H_2O_2 in Bioclean water with the lowest LOD of 0.08 μM among the tetrapyrrole-modified H_2O_2 sensors reported thus far.[9]

For most applications, the structures of solid films have a crucial effect on the performances of the molecular devices.[25] Thus far, toward their future practical applications a variety of porphyrin and phthalocyanine thin films have been fabricated using vacuum deposition technique and in particular the solution-based processes such as solution casting (e.g., drop-casting and spin-coating) and layer-by-layer assembly including LB (Langmuir−Blodgett), LS (Langmuir−Shäfer), and QLS (quasi-Langmuir−Shäfer) methods. Among the solution-based methods, the solution casting technique is surely appealing for large-scale and low-cost processing, in which however it is difficult to accurately control film thickness due to the uneven distribution of nanostructures on a solid substrate. In contrast, both LB and LS methods can afford multilayer structured membranes with precise thickness control for amphiphilic phthalocyanine/porphyrin compounds.[26] However, the irrelatively complicated operation procedure requiring the necessary help of corresponding apparatus rendered the recent relatively wide application of newly developed QLS technique without using any sophisticated apparatus toward the fabrication of well-organized molecular films at air−water interface.[14]

Inspired by various excellent functional properties revealed for the well-known two-dimensional (2D) carbon material, graphene,[20−23] and the rich electrochemical and semiconductive properties of sandwich porphyrinato and/or phthalocyaninato rare earth compounds,[27−32] we developed a facile method for fabricating the multilayer hybrid films of a mixed (phthalocyaninato) (porphyrinato) europium(III) triple-decker compound (Pc)Eu(Pc)Eu[*trans*-T($COOCH_3$)$_2$PP] (**1**) and graphene oxide (GO) (Scheme 1), using the solution-based QLS technique. The combined features offered by nanocomposite of GO and triple-decker components are expected to provide nonenzymatic H_2O_2 electrochemical sensors with excellent stability, reproducibility, and selectivity.

Scheme 1. Schematic Molecular Structures of (Pc)Eu(Pc)Eu[*trans*-T($COOCH_3$)$_2$PP] (1) and Graphene Oxide (GO)

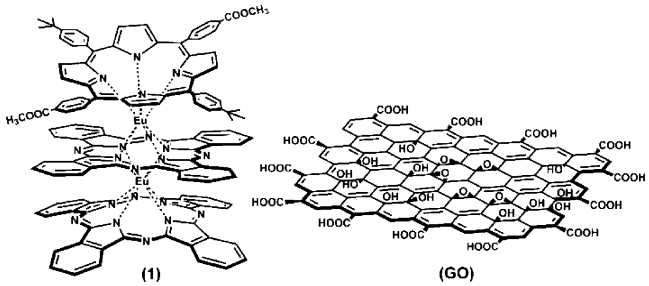

RESULTS AND DISCUSSION

Synthesis and Electrochemistry of 1. In order to get the targeted electroactive triple-decker with proper HOMO and LUMO energies, good solubility, and good film-forming ability at the air/water interface, two di(4-methoxylcarbonylphenyl) groups and two di(4-*tert*-butylphenyl) substituents were introduced onto the opposite meso-positions of the porphyrin chromophore, respectively, resulting in a novel semiconducting triple-decker (Pc)Eu(Pc)Eu[*trans*-T($COOCH_3$)$_2$PP] (**1**) [Pc = dianion of phthalocyanine; *trans*-T($COOCH_3$)$_2$PP = dianion of 5,15-di(4-methoxylcarbonylphenyl)-10,20-di(4-*tert*-butylphenyl)porphyrin, Scheme 1].[33] It is worth noting that introduction of the methoxylcarbonyl substituents onto the periphery of porphyrin ring in the triple-decker compound also provides sufficient active sites to interact with the oxygenous (such as carboxylic, hydroxyl, and epoxy) groups on the surface of GO in a noncovalent manner. This new triple-decker was confirmed by MALDI-TOF and ^{1}H NMR as detailed in Figures S1 and S2.

The electrochemical characteristic of triple-decker **1** was assessed by differential pulse voltammetry (DPV) analysis. As shown in Figure 1, complex **1** in CH_2Cl_2 shows six reversible

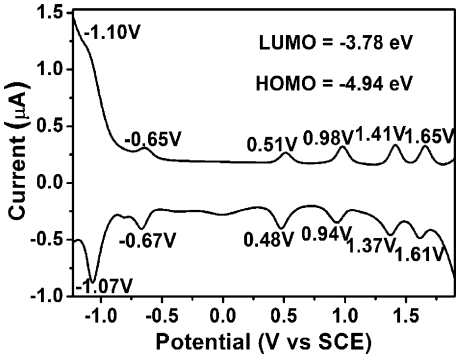

Figure 1. Differential pulse voltammetry (DPV) of **1**.

single-electron redox processes with the first oxidation occurring at +0.50 V (vs SCE), and first reduction at −0.66 V (vs SCE) (Figure 1 and Table S1). Its HOMO and LUMO energies are calculated to be −4.94 and −3.78 eV, respectively, according to $E_{HOMO} = -E_{1/2}^{oxd1} - 4.44$ eV and $E_{LUMO} = -E_{1/2}^{red1} - 4.44$ eV,[34] ensuring its good ambipolar (p- and n-type) organic semiconducting nature.[35] Obviously, the narrow band gap (ΔE) of 1.16 eV in combination with the wide redox potential range suggests good electrochemical catalytic properties of this triple-decker compound with application potential in electrochemical sensors.[2,24]

Morphologies and Internal Structures of Triple-Decker/GO and Triple-Decker QLS Nanostructured Films. Figure 2 compares the morphologies of the GO film, triple-decker QLS film, and triple-decker/GO hybrid film deposited on SiO_2 substrates. As shown in Figure 2A, the GO film exhibited the sheetlike structure, and a root-mean-square (R_{rms}) roughness of 0.6 nm was obtained, which agrees with a typical one-atom-thick graphene oxide thickness (ca. 0.9 nm).[36,37] The surface of the triple-decker QLS film exhibits a randomly dispersed aggregate domains (ca. 100−500 nm in

DOI: 10.1021/acsami.6b08760
ACS Appl. Mater. Interfaces XXXX, XXX, XXX−XXX

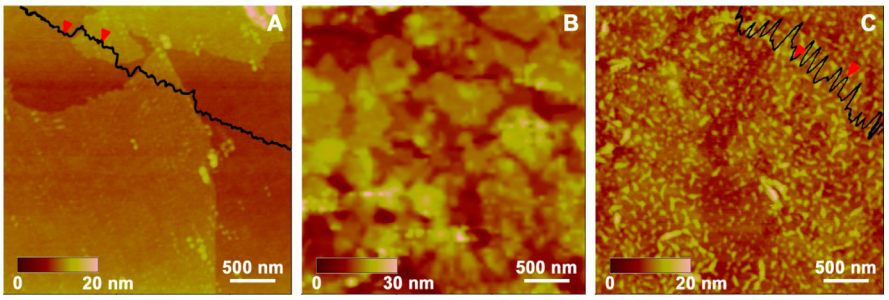

Figure 2. AFM images of GO (A), triple-decker QLS film (B), and triple-decker/GO hybrid film (C). The line scans in A and C show the apparent height of GO sheet (0.9 nm) and hybrid film (2.5 nm), respectively.

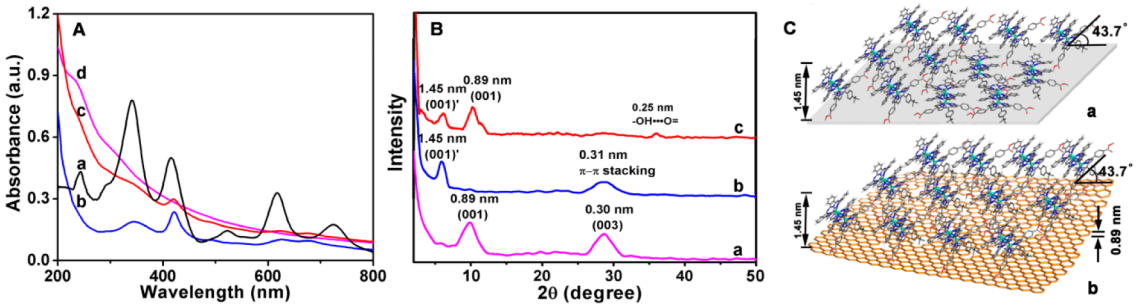

Figure 3. (A) Electronic absorption spectra of triple-decker **1** in $CHCl_3$ solution (a), pure triple-decker QLS film (b), hybrid triple-decker/GO QLS film (c), and GO film (d). (B) Out-of-plane (OOP) X-ray diffraction (XRD) patterns for pure GO film (a), triple-decker QLS film (b), and triple-decker/GO hybrid film (c) deposited on bare SiO_2/Si substrate together with (C) the schematic packing mode of the triple-decker molecules in pure triple-decker QLS film (a) and hybrid film (b).

diameter) with somewhat large gaps and cracks between domains and a R_{rms} value as high as 2.8 nm (Figure 2B). However, after being fabricated onto the GO surface, uniform granular crystallites (ca. 70 nm in diameter) significantly diminished grain boundaries were observed for the triple-decker aggregates (Figure 2C), revealing the highly optimized film structure and morphology in the triple-decker/GO hybrid film. The thickness of ca. 2.5 nm for the triple-decker/GO film confirms its hybrid film nature with triple-decker aggregate being formed on the GO surface.[36] It is believed that the oxygenous groups such as carboxylic, hydroxyl, and epoxy groups distributed over GO surface play a key role for the formation of uniformly sized nanostructures of triple-decker in the hybrid film: GO binds the first layer of triple-decker molecules via hydrogen bonding interaction between the porphyrin-$COOCH_3$ groups and GO carboxylic/hydroxyl groups, which as the active centers induce further self-orgnization of triple-decker molecules depending on effective $\pi-\pi$ interaction between triple-decker molecules and resulting in uniform granular crystallites (Figure 2C) rather than the randomly dispersed aggregate domains in pure triple-decker QLS film. In addition, the significantly diminished grain boundaries among the uniformly sized aggregates in the hybrid film will be surely helpful in improving the charge transport capacity, electrocatalytic activity, supramolecular recognition, and enrichment ability of the triple-decker aggregates for electrochemical sensing applications.[38] It is noteworthy that the surface morphology of the GO film, triple-decker QLS film, and triple-decker/GO hybrid film were also examined by SEM technique (Figure S3), and the results agree well with those procured by AFM observation.

In order to understand the molecular packing mode of triple-decker molecules and the internal film structure, electronic absorption, and polarized UV−vis spectroscopic and thin-film XRD measurements have been conducted for both pure and hybrid QLS films, Figure 3. As shown in Figure 3A, (Pc)Eu(Pc)Eu[*trans*-T($COOCH_3$)$_2$PP] in $CHCl_3$ solution displays intense Soret bands at 342 and 415 nm, respectively, and Q absorptions at 616 and 726 nm with one weak vibrational shoulder at 523 nm[33,39] in addition to a weak L band at 244 nm arising from a forbidden $\pi-\pi^*$ transition of the benzene moieties.[40] After being fabricated into the QLS film (Figure 3A), the two Soret bands red-shift from 342 to 346 nm and from 415 to 420 nm, respectively, while one Q absorption red-shifts from 616 to 626 nm and the other at 726 blue-shifts to 678 nm. These imply that the molecules of **1** take a slipped "face-to-face" stack and "edge-on" orientation in the QLS film of **1**.[13,41−43] The similar "slipped cofacial" molecular packing of **1** was also observed in the triple-decker/GO hybrid film (Figure 3A). Further evidence was derived from the orientation angle (dihedral angle) of the tetrapyrrole rings with respect to the surface of substrate, 43 and 47° for the pure and hybrid film, respectively, on the basis of the polarized UV−vis spectroscopic measurement result[44] (Figure S4 and Table S2). It is noteworthy in the electronic absorption spectrum of GO film shown in Figure 3A that two characteristic absorption bands at ca. 300 and 237 nm emanating from n−π^* and $\pi-\pi^*$ transitions of the C═O and C═C band, respectively, were clearly observed.[45,46] Similar absorptions were also found in the hybrid film but not in the pure triple-decker QLS film. Nevertheless, along with the increase in the energy from 800 to 200 nm, the absorption intensity for the hybrid film gets increased in a way similar to that of the GO film, confirming the hybrid nature of the triple-decker/GO film.

Figure 3B shows the out-of-plane (OOP) X-ray diffraction (XRD) patterns of the three kinds of membranes deposited on

DOI: 10.1021/acsami.6b08760
ACS Appl. Mater. Interfaces XXXX, XXX, XXX−XXX

SiO_2/Si substrate. In the XRD diagram of the GO film shown in Figure 3B, two well-defined diffraction peaks at 2θ = 9.95 and 28.7° attributed to the diffractions from the (001) and (003) planes, respectively, corresponding to a mean interlayer spacing of 0.9 nm typical for GO,[47,48] were observed. This result is consistent with that derived from the AFM observation as detailed above. The pure triple-decker QLS film displays a typical (001) diffraction peak at 1.45 nm (2θ = 6.24°), which corresponds to a periodic spacing distance between two neighbor molecules of **1** along the direction of the substrate surface normal (Figure 3B). On the basis of the energy-optimized molecular structure,[39,49,50] the diagonal dimension of the triple-decker **1** is ca. 2.1 nm (Figure S5). Consequently, the orientation angle between the tetrapyrrole ring of **1** and substrate surface was estimated to be ca. 43.7° (Figures 3C), corresponding well with the UV−vis and polarized UV−vis spectroscopic results and confirming the formation of *J* aggregates with an "edge-on" conformation of the molecules of **1** in the QLS film.[39,49,51] In addition, a higher-order diffraction observed at 2θ = 28.72° (d = 0.31 nm) for the pure triple-decker QLS film is assigned to the stacking distance among tetrapyrrole rings of triple-decker molecules with face-on orientation (Figure 3C).[52−54] In the XRD pattern of the triple-decker/GO hybrid film shown in Figure 3B, observation of two peaks at 2θ = 6.22° (d = 1.45 nm) and 2θ = 10.06° (d = 0.89 nm) corresponding to the (001) lattice planes of the triple-decker and GO layers, respectively, suggests the regular layered structure and the same molecular stacking structure employed by the triple-decker molecules and GO in the hybrid film as in corresponding single-component films. The fact that only the (00l) diffraction peak of triple-decker is observed, in combination with the lack of the stacking peak in the OOP XRD diagram of the hybrid film, suggests the identical edge-on orientation employed by the triple-decker molecules on the substrate (Figure 3C).[52,55,56] Actually, the hybrid film XRD pattern also shows an additional diffraction at 0.25 nm, which is attributed to the intermolecular hydrogen bonding formed between the carbonyl groups of the molecules of **1** and hydroxyl/carboxyl groups of GO.[33] Obviously, as a result of the self-assembly of the molecules of **1** over the GO surface depending on the noncovalent hydrogen bonding interactions, the molecular packing mode for the triple-decker changes from both the edge-on and face-on configurations in pure QLS film to the identical edge-on one in the hybrid film (Figure 3C), indicating the template role of GO for the aggregation of triple-decker molecules. This, together with the great surface area of conductive GO, is responsible for the excellent electrocatalytic activity of the triple-decker/GO hybrid film-based electrochemical sensors (*vide infra*).

Electrochemical Characterization of the Triple-Decker/GO Hybrid Film and Triple-Decker QLS Film. To investigate the electrochemical response of the newly developed hybrid film, cyclic voltammograms (CVs) were registered in phosphate buffer (PBS, pH 7.3) for the bare ITO electrode, ITO covered with the GO film (GO/ITO), pure triple-decker QLS film (triple-decker/ITO), and hybrid film (triple-decker/GO/ITO), respectively. As shown in Figure 4, the bare ITO electrode does not exhibit any notable response, while the GO-covered ITO electrode displays a couple of small redox peaks appearing at 0.35 and 0.65 V assigned to the oxygenous groups on the surface of GO,[57] and the triple-decker QLS film-covered ITO electrode exhibits two redox couples with the cathodic peaks at 0.10 and 0.61 V due to the {triple-decker}/{triple-decker}$^-$ and {triple-decker}/{triple-decker}$^+$ redox process, respectively.[58,59] In addition, GO/ITO shows a higher background current than triple-decker/ITO, disclosing a better electron transfer nature of the former electrode than the latter one. Furthermore, the background current for the ITO electrode covered by triple-decker/GO hybrid film was significantly enhanced due to the enhanced electron transport associated with the improved semiconducting triple-decker molecular ordering on the GO sheet with intrinsic good conductivity. The result in the observation of an additional cathodic peak at −0.45 V should be assigned to the {triple-decker}/{triple-decker}$^{2-}$ process.[60,61] These results clearly indicate the better performance of the triple-decker/GO/ITO electrode in affording a high signal-to-background ratio peak current than the single-component (either GO or triple-decker) film-modified ITO electrodes. Additionally, the $I-V$ measurements for the GO film, triple-decker QLS film, and triple-decker/GO hybrid film were also carried out (Figure S6). The conductivity is therefore calculated to amount to 2.04×10^{-4} S cm^{-1} for the GO film, 2.63×10^{-6} S cm^{-1} for the QLS film, and 3.61×10^{-4} S cm^{-1} for the triple-decker/GO hybrid film, respectively.[14] Compared with the triple-decker QLS film, the conductivity of the triple-decker/GO hybrid film was significantly improved due to the relatively high intrinsic conductivity of GO together with the more effective $\pi-\pi$ stacking among adjacent triple-decker molecules within the uniform nanosized aggregates formed in the hybrid film associated with the induced effect of GO template as revealed by XRD and AFM analysis.

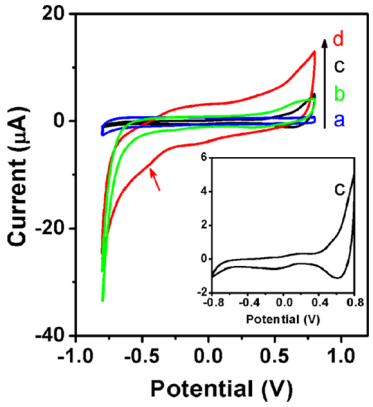

Figure 4. CVs of bare ITO (a), GO/ITO (b), triple-decker/ITO (c), and triple-decker/GO/ITO (d) in PBS solution (pH 7.3) at a scan rate of 0.02 V s^{-1}.

Direct Detection of H_2O_2 at the Triple-Decker/GO/ITO Electrode. For revealing the electrochemical activity of the triple-decker/GO hybrid film to H_2O_2, the CVs of the bare ITO electrode, GO/ITO electrode, and triple-decker/GO/ITO electrode (covered with 35-layer of hybrid film) were comparatively studied in 0.1 mM H_2O_2 solution. As can been seen in Figure 5, no significant change in the current of the peaks could be revealed for both bare ITO and GO/ITO electrodes in comparison with those in the absence of H_2O_2 shown in Figure 4, indicating the lack of any electrochemical reduction of these two electrodes over H_2O_2. Interestingly, despite the lack of any change in the current for the peaks at −0.02 and −0.1 V, the current for the peak at ca. −0.45 V in 0.1 mM H_2O_2 for the triple-decker/GO/ITO electrode gets significantly increased in comparison with that in the absence of H_2O_2, as shown in the inset of Figure 5, indicating the

DOI: 10.1021/acsami.6b08760
ACS Appl. Mater. Interfaces XXXX, XXX, XXX−XXX

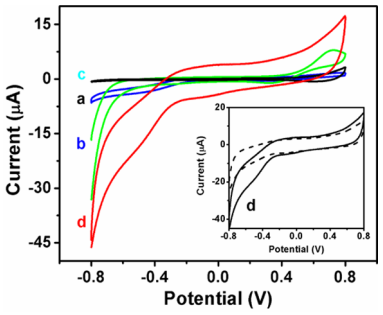

Figure 5. CVs of bare ITO (a), GO/ITO (b), triple-decker/ITO (c), and triple-decker/GO/ITO (d) electrode recorded in PBS (pH 7.3) with 0.1 mM H_2O_2 at the scan rate of 0.02 V s^{-1}. The inset is the CVs of triple-decker/GO/ITO electrode before (dashed line) and after (solid line) addition of 0.1 mM H_2O_2.

effective reduction of the hybrid film-modified electrode toward H_2O_2 at this reduction potential. Increase in the active sites and improvement in the triple-decker semiconductivity associated with the well-distributed small and uniformed-sized triple-decker nanodomains on the GO surface as mentioned above, in combination with the intrinsic good conductivity of the GO itself, should be responsible for the enhanced electrochemical activity of the hybrid film over the pure triple-decker film.

To unravel the charge-transporting characteristics of the hybrid film, the CVs of triple-decker/GO/ITO electrode were studied under various scan rates from 0.01 to 0.1 V s^{-1} with 0.01 interval in PBS (pH 7.3) with the concentration of H_2O_2 being kept at 0.1 mM. As shown in Figure 6, the reduction peak

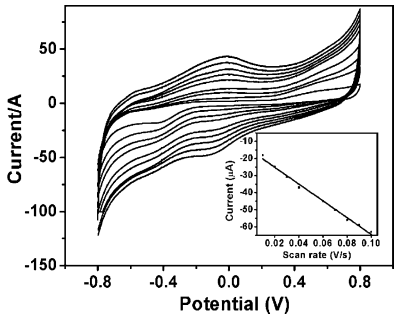

Figure 6. Change in CV of 0.1 mM H_2O_2 in PBS solution (pH 7.3) at triple-decker/GO/ITO electrode in the scan rates ranged from 0.01 to 0.02, 0.03, 0.04, 0.06, 0.07, 0.08, 0.09, and 0.1 V s^{-1}. Inset: plot of the reduction peak currents at −0.45 V vs the scan rates.

currents at −0.45 V exhibited a linear dependence on scan rates (correlation coefficient = 0.991), clearly revealing the surface-confined process of this reduction process.[2] In addition, the position for the reduction peak at −0.45 V remained unchanged with the scan rates ranging from 0.01 to 0.1 V s^{-1}, suggesting the excellent redox ability and fast charge transfer dynamics of the triple-decker molecules at the hybrid film-modified electrode.[2] This is also true for the redox couple with E_{pa} and E_{pc} at −0.02, and −0.10 V, respectively, due to the {triple-decker}/{triple-decker}$^-$ process.

To achieve the best performance for the detection of H_2O_2, CVs of triple-decker/GO/ITO electrode with different layers of hybrid film were recorded in the applied potential from −0.8 to 0.8 V in PBS solution (pH 7.3) with 0.1 mM of H_2O_2 at the scan rate of 0.02 V s^{-1}. The current of the reduction peak at −0.45 V changes, obviously depending on the number of the hybrid film layer modified onto the ITO electrode (Figures 7A and S7), with the highest response being achieved at a 35-layer hybrid film modified ITO electrode. In addition, amperometric measurement over the 35-layer hybrid film modified ITO electrode was carried out under different applied potential, Figure 7B, confirming the optimum applied potential of −0.45 V for H_2O_2 detection.

On the basis of the above-described result, the sensing property of the 35-layer hybrid film-modified ITO electrode (triple-decker/GO/ITO) toward H_2O_2 was then determined by means of the chronoamperometry method at −0.45 V. Figure 7C exhibits the response curve of steady-state current−time (I−t) for the triple-decker/GO/ITO electrode to the successive addition of H_2O_2. Obviously, the hybrid film-modified electrode responded quite quickly to the addition of H_2O_2, and the catalytic current achieved ca. 95% of the maximum steady-state current within 2.5 s upon every injection of H_2O_2, indicating the high electron transfer efficiency and fast diffusion of H_2O_2 onto the electrode surface.[62] In particular, the catalytic current (I) increases in a linear manner depending on the concentration (c) of H_2O_2 with the calibration plot (I vs c) of I (μA) = −0.173−0.0074c (μM) (R^2 = 0.996) in the range of 0.05−8.5 μM and I (μA) = −0.231−0.00039c (μM) (R^2 = 0.992) in the range of 8.5−1800 μM shown in Figure 7D, representing the widest range with linear current−concentration relationship reported thus far for the H_2O_2 detection using nonenzymatic electrochemical sensors (Table S3). In addition, the limit of detection (LOD) of the present H_2O_2 sensor was calculated to be 17 nM (3 × SB/slope),[59] again representing the best result reported thus far for tetrapyrrole-modified nonenzymatic H_2O_2 sensors (Table S3). It is noteworthy that the large slope of the calibration curve revealed for the hybrid film-based electrode toward H_2O_2 detection at the concentration lower than 8.5 μM seems to indicate that the adsorption of H_2O_2 onto the hybrid film dominates the H_2O_2-detecting procedure in the system at low H_2O_2 concentration range. Along with the enhancement of H_2O_2 concentration, the diffusion of H_2O_2 at the surface of electrode changes to be the dominant step of the whole procedure, which in turn results in a decreased linear relationship slope in the H_2O_2 concentration range higher than 8.5 μM.[63]

Interference Study, Stability, and Reproducibility. The influence of potential interferents on the determination of H_2O_2 was assessed by the chronoamperometry method at −0.45 V for a 35-layer hybrid film-modified ITO electrode.[64] As shown in Figure 8A, the current gets obviously increased along with the injection of 0.01 mM H_2O_2 into PBS solution (pH 7.3). However, addition of 0.01 mM L-tryptophan (L-Try), L-arginine (L-Arg), glucose (Glu), ascorbic acid (AA), and dopamine (DA) does not induce any change in the current, while adding 0.01 mM L-histidine (L-His), citric acid (CA), and saturated oxygen (O_2) only leads to a negligible current increase, indicating the noninterference nature of these substances and the high selectivity of triple-decker/GO/ITO electrode for H_2O_2 detection.

For assessing stability of the triple-decker/GO/ITO electrode, its current response to 0.1 mM H_2O_2 in PBS solution (pH 7.3) was recorded every 2 days by CV. As revealed in Figure 8B, the peak current at −0.45 V was lowered to ca. 90.3% of its primary value after 8 days, implying the relatively high stability of the electrodes in air. Nevertheless, the operational stability of the newly developed triple-decker/GO/

DOI: 10.1021/acsami.6b08760
ACS Appl. Mater. Interfaces XXXX, XXX, XXX−XXX

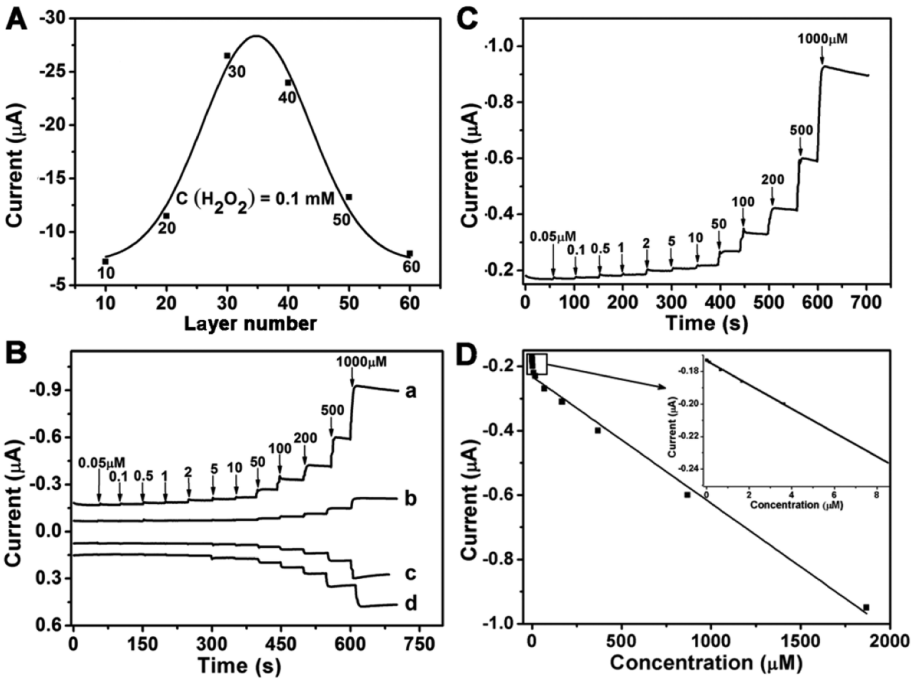

Figure 7. (A) Plot of the current for the cathodic peak at −0.45 V vs the number of hybrid film layer at the ITO surface recorded by CVs at 0.02 V s^{-1} in PBS solution (pH 7.3) with 0.1 mM H_2O_2. (B) Current−time (I−t) curves of triple-decker/GO/ITO electrode at applied potential of −0.45 V (a), − 0.1 V (b), − 0.01 V (c), and 0.65 V (d) with successive injection of a series of concentration of H_2O_2 into PBS solution (pH 7.3). (C) Amperometric response of the triple-decker/GO/ITO electrode to successive injection of H_2O_2 at −0.45 V and (D) corresponding calibration plots for the triple-decker/GO/ITO electrode. Inset: Plot for the H_2O_2 concentration range of 0.05−8.5 μM.

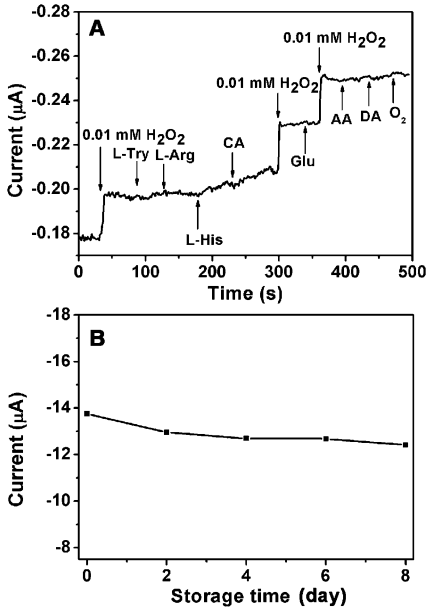

Figure 8. (A) Amperometric response recorded for the triple-decker/GO/ITO electrode on successive addition of 0.01 mM H_2O_2 followed by addition of 0.01 mM L-tryptophan (L-Try), L-arginine (L-Arg), L-histidine (L-His), citric acid (CA), glucose (Glu), ascorbic acid (AA), dopamine (DA), and saturated oxygen (O_2) in PBS solution of pH 7.3. (B) Variation of the current of the peak at −0.45 V from CVs for the triple-decker/GO/ITO electrode in PBS solution (pH 7.3) with 0.1 mM H_2O_2 along with the storage time.

ITO electrode was further investigated by the amperometric current−time technique at the optimized potential of −0.45 V. Successive determination of 0.01 mM H_2O_2 for 30 min induces only ca. 5.8% decrease in the peak current, which is still sensitive toward 0.01 mM H_2O_2 (Figure S8), indicating the good operational stability of this hybrid film electrode. In addition, AFM measurement was also conducted for the 35-layer hybrid film after detection (Figure S9). As can be seen, the 35-layer hybrid film still shows the uniform granular crystallites with a diameter of ca. 50−70 nm at the surface of GO sheets, almost the same as that before detection (Figure 2C), giving further evidence for electrode stability after detection. In addition, to evaluate the reproducibility of the triple-decker/GO/ITO electrode, amperometric current−time measurement was repeated five times for one electrode, achieving a RSD (relative standard deviation) value for the current response of less than 6.3%. In a similar manner, corresponding measurement over five triple-decker/GO/ITO electrodes leads to the RSD value of less than 5.0%, confirming the excellent reproducibility of the electrode toward H_2O_2 sensing.

Practicality of the Triple-Decker/GO/ITO Electrode. To evaluate the application potential of the triple-decker/GO/ITO electrode in practical food monitoring and clinical diagnosis, measurement of H_2O_2 in a series of natural samples including milk, beer, fetal calf serum, and human urine using the newly developed hybrid film electrode was studied by the current−time (I−t) method at the optimized voltage of −0.45 V. It is worth noting that the milk and beer samples were purchased from the market, fetal calf serum obtained from Tianjin Haoyang biotechnology Co, Ltd., and human urine collected from volunteers of two males and two females aged 23−27 years without any pretreatment. To get the medium for electrochemical measurement, each sample was diluted by PBS solution (pH 7.3) with a volume ratio of 1:9 (sample/PBS solution), and the determination of H_2O_2 in real samples was performed with the help of a standard addition method

DOI: 10.1021/acsami.6b08760
ACS Appl. Mater. Interfaces XXXX, XXX, XXX−XXX

Table 1. Determination of H_2O_2 in Real Samples[a]

samples	added (μM)	found (μM)	recovery (%)	RSD (%)	samples	added (μM)	found (μM)	recovery (%)	RSD (%)
milk	0	0.16		3.7	fetal calf serum	0	0.33		4.7
	1.0	1.12	96.0	4.2		1.0	1.21	95.0	3.6
	5.0	5.11	99.0	5.3		5.0	5.29	99.2	5.2
	10.0	10.22	100.6	4.3		10.0	10.41	100.8	4.2
beer	0	0.49		7.9	urine	0	0.28		6.0
	1.0	1.48	99.0	5.4		1.0	1.27	99.0	3.9
	5.0	5.60	102.2	7.1		5.0	5.49	104.2	4.0
	10.0	10.13	96.4	8.7		10.0	10.71	104.4	4.1

[a] $n = 4$.

(actually by adding the standard concentrations of H_2O_2 into the previously N_2-saturated real samples).[65] As shown in Table 1, the recoveries are ranging from 95 to 104%, demonstrating the good practicability of the newly developed electrochemical sensor.

CONCLUSIONS

An efficient nonenzymatic H_2O_2 electrochemical sensor has been developed based on the hybrid film of (Pc)Eu(Pc)Eu[*trans*-T(COOCH$_3$)$_2$PP] triple-decker semiconductor with GO using a simple QLS method for the first time. The triple-decker/GO/ITO sensor exhibited the best performance among the tetrapyrrole-modified nonenzymatic electrochemical sensors for H_2O_2 in terms of low LOD, a larger linear concentration range, fast response, high stability, and good selectivity and reproducibility. The present result provides a promising strategy toward developing nonenzymatic electrochemical sensors with a wide range of application potentials.

EXPERIMENTAL SECTION

Graphite powder and H_2O_2 (30%) were purchased from Aladdin Co, Ltd. KCl, $Na_2HPO_4{\cdot}12H_2O$, and KH_2PO_4 were obtained from Sinopharm Chemical Reagent Company, Ltd. (Shanghai, China). All reagents and solvents are at least analytical-grade and used as received. Phosphate-buffered solution (PBS, pH 7.3), as the solvent of analytes, was made from 0.1 M KCl mixed with 0.01 M KH_2PO_4 and 0.04 M $Na_2HPO_4{\cdot}12H_2O$ aqueous solution prepared in deionized water (resistivity of 18.2 MΩ cm^{-1}). Graphene oxide (GO) is prepared as descripted in the literature.[66,67] Details are included in the Supporting Information on the preparation procedure, powder XRD pattern (Figure S10), and film SEM images of GO (Figure S11).

The UV−vis spectra were recorded on a Hitachi U3900 spectrophotometer. XRD patterns were recorded on a Bruker D8 FOCUS X-ray diffractometer. AFM images were obtained under ambient conditions using the tapping mode with a NanoscopeIII/Bioscope scanning probe microscope from digital instruments. Electrochemical experimental measurements for the sensors were studied on a CHI760D electrochemical workstation. Platinum plate and Hg/Hg_2Cl_2 electrodes (saturated solution of KCl) were used as counter and reference electrodes, respectively. The newly modified ITO electrode was employed as the working electrode with a geometric working of 1.4 cm^2. CVs were performed in PBS solution (pH 7.3). Before all electrochemical experiments, PBS solution was purified by high-purity N_2 gas for 15 min to remove the dissolved oxygen, and the nitrogen atmosphere was maintained throughout the measurement procedure at room temperature. Current−time (I−t) curves were recorded in PBS solution (pH 7.3). Current−voltage (I−V) curves were measured in the applied voltage range from −10 to 10 V with steps of 0.05 V. The detail parameters of interdigitated electrode (IDE) array used were as the same as those in our previous report.[14]

Preparation of (Pc)Eu(Pc)Eu[*trans*-T(COOCH$_3$)$_2$PP] (1). The triple-decker complex (Pc)Eu(Pc)Eu[*trans*-T(COOCH$_3$)$_2$PP] (**1**) was synthesized as descripted in our previous published procedures.[27,30,33,68] The detailed procedures were presented in the Supporting Information. ^{1}H NMR (400 MHz, $CDCl_3$, δ) 12.64 (d, 2H, Por-*t*-butyl-Ph-H$_o^{endo}$), 11.84 (s,16H, Pc$_{in}$−H), 10.07 (d, 2H, Por-*t*-carbomethoxy-Ph-H$_o^{exo}$), 9.81 (d, 2H, Por-*t*-carbomethoxy-Ph-H$_o^{endo}$), 9.13 (d, 2H, Por-*t*-butyl-Ph-H$_o^{exo}$), 7.52 (s, 16H, Pc$_{out}$−H), 6.67 (d, 2H, Por-*t*-butyl-Ph-H$_m^{endo}$), 5.24 (d, 2H, Por-*t*-butyl-Ph-H$_m^{exo}$), 4.79 (d, 2H, Por-*t*-carbomethoxy-Ph-H$_m^{exo}$), 4.47 (s, 6H, −COOCH$_3$), 4.43 (d, 2H, Por-*t*-carbomethoxy-Ph-H$_m^{endo}$), 2.64 (s, 8H, Por-H$_\beta$), 1.93 (s, 18H, *t*-butyl); MALDI-TOF MS: an isotopic cluster peaking at m/z 2171, Calcd for $C_{120}H_{80}Eu_2N_{20}O_4$, [M]$^+$, 2170.

Preparation of Triple-Decker/GO and Triple-Decker QLS Nanostructured Films. Prior to deposition, substrates were successively washed by deionized water, alcohol, and CH_2Cl_2 in ultrasound bath. Films were deposited on Si/SiO_2, quartz, and ITO substrates by using the quasi-Langmuir−Shäfer (QLS) self-assembly method.[16,39] Briefly, the solution of (Pc)Eu(Pc)Eu[*trans*-T(COOCH$_3$)$_2$PP] (**1**) in CH_2Cl_2 (~1 × 10^{-5} M, 5.0 mL) was put into a glass culture dish (with diameter of 9.5 cm, height of 1.5 cm, and volume of 106 mL); then, the yellow-brown solution of GO in ultrapure water (0.1 mg/mL, 65 mL)[69] was dropwise added onto the surface of the triple-decker solution until 95% of the surface of organic solution had been covered by GO aqueous solution. Along with the evaporation of solvent, the self-assembled nanostructures of the triple-decker molecules gradually formed on the surface of GO solution and thus formed a densely packed film. The resulting film can be easily transferred to a substrate by horizontal lifting method. This procedure was repeated to get the multilayer film. For comparative study, QLS film of (Pc)Eu(Pc)Eu[*trans*-T(COOCH$_3$)$_2$PP] itself was also fabricated with ultrapure water instead of the GO solution as subphase.

ASSOCIATED CONTENT

Supporting Information

The Supporting Information is available free of charge on the ACS Publications website at DOI: 10.1021/acsami.6b08760.

Synthesis and characterization details of triple-decker **1** and GO; SEM patterns, I−V curves and polarized UV−vis spectra of the films; energy-optimized molecular structure of (Pc)Eu(Pc)Eu[*trans*-T(COOCH$_3$)$_2$PP]; CVs of different hybrid film layers; operational stability of the triple-decker/GO/ITO electrode and the AFM image of hybrid film with 35 layers after the detection; comparison table of different H_2O_2 sensors for the determination of H_2O_2 (PDF)

AUTHOR INFORMATION

Corresponding Authors

*E-mail: yanlichen@upc.edu.cn.
*E-mail: jianzhuang@ustb.edu.cn.

Notes

The authors declare no competing financial interest.

DOI: 10.1021/acsami.6b08760
ACS Appl. Mater. Interfaces XXXX, XXX, XXX−XXX

■ ACKNOWLEDGMENTS

This work was financially supported by the National Natural Science Foundation of China (Nos. 21371073 and 21290174) and the National Key Basic Research Program of China (Nos. 2013CB933402 and 2012CB224801).

■ REFERENCES

(1) Zhu, M.; Li, N.; Ye, J. Sensitive and Selective Sensing of Hydrogen Peroxide with Iron-Tetrasulfophthalocyanine-Graphene-Nafion Modified Screen-Printed Electrode. *Electroanalysis* **2012**, *24*, 1212−1219.

(2) Bai, J.; Jiang, X. A Facile One-Pot Synthesis of Copper Sulfide-Decorated Reduced Graphene Oxide Composites for Enhanced Detecting of H_2O_2 in Biological Environments. *Anal. Chem.* **2013**, *85*, 8095−8101.

(3) Hurdis, E. C.; Romeyn, J. H. Accuracy of Determination of Hydrogen Peroxide by Cerate Oxidimetry. *Anal. Chem.* **1954**, *26*, 320−325.

(4) Nogueira, R. F. P.; Oliveira, M. C.; Paterlini, W. C. Simple and Fast Spectrophotometric Determination of H_2O_2 in Photo-Fenton Reactions Using Metavanadate. *Talanta* **2005**, *66*, 86−91.

(5) Zhu, X.; Niu, X.; Zhao, H.; Lan, M. Doping Ionic Liquid into Prussian Blue-Multiwalled Carbon Nanotubes Modified Screen-Printed Electrode to Enhance the Nonenzymatic H_2O_2 Sensing Performance. *Sens. Actuators, B* **2014**, *195*, 274−280.

(6) Hu, Y.; Zhang, Z.; Yang, C. The Determination of Hydrogen Peroxide Generated from Cigarette Smoke with An Ultrasensitive and Highly Selective Chemiluminescence Method. *Anal. Chim. Acta* **2007**, *601*, 95−100.

(7) Wang, J. Electrochemical Biosensors: Towards Point-of-Care Cancer Diagnostics. *Biosens. Bioelectron.* **2006**, *21*, 1887−1892.

(8) Gorton, L.; Bremle, G.; Csöregi, E.; Jönsson-Pettersson, G.; Persson, B. Amperometric Glucose Sensors Based on Immobilized Glucose-Oxidizing Enzymes and Chemically Modified Electrodes. *Anal. Chim. Acta* **1991**, *249*, 43−54.

(9) Park, S.; Singh, A.; Kim, S.; Yang, H. Electroreduction-Based Electrochemical-Enzymatic Redox Cycling for the Detection of Cancer Antigen 15−3 Using Graphene Oxide-Modified Indium−Tin Oxide Electrodes. *Anal. Chem.* **2014**, *86*, 1560−1566.

(10) Itaya, K.; Shoji, N.; Uchida, I. Catalysis of the Reduction of Molecular Oxygen to Water at Prussian Blue Modified Electrodes. *J. Am. Chem. Soc.* **1984**, *106*, 3423−3429.

(11) Li, L.; Zhang, X.; He, X.; Lu, W.; Yang, L.; Bian, Y.; Weng, Y.; Jiang, J. C_{60}-Modified Mixed (Phthalocyaninato) (Porphyrinato) Yttrium(III) Double-Decker Complex: Synthesis, Characterization, and Photophysical Properties. *Dyes Pigm.* **2014**, *102*, 257−262.

(12) Chen, W.; Cai, S.; Ren, Q.; Wen, W.; Zhao, Y. Recent Advances in Electrochemical Sensing for Hydrogen Peroxide: a Review. *Analyst* **2012**, *137*, 49−58.

(13) Chen, Y.; Su, W.; Bai, M.; Jiang, J.; Li, X.; Liu, Y.; Wang, L.; Wang, S. High Performance Organic Field-Effect Transistors Based on Amphiphilic Tris(phthalocyaninato) Rare Earth Triple-Decker Complexes. *J. Am. Chem. Soc.* **2005**, *127*, 15700−15701.

(14) Chen, Y.; Bouvet, M.; Sizun, T.; Gao, Y.; Plassard, C.; Lesniewska, E.; Jiang, J. Facile Approaches to Build Ordered Amphiphilic Tris(Phthalocyaninato) Europium Triple-Decker Complex Thin Films and Their Comparative Performances in Ozone Sensing. *Phys. Chem. Chem. Phys.* **2010**, *12*, 12851−12861.

(15) Doyle, J. J.; Ballesteros, B.; de la Torre, G.; McGovern, D. A.; Kelly, J. M.; Torres, T.; Blau, W. J. Combination of Phthalocyanine and Fullerene Moieties for Optical Limiting. *Chem. Phys. Lett.* **2006**, *428*, 307−311.

(16) Gay Martín, M.; de Saja, J. A.; Munoz, R.; Rodríguez-Méndez, M. L. Multisensor System Based on Bisphthalocyanine Nanowires for the Detection of Antioxidants. *Electrochim. Acta* **2012**, *68*, 88−94.

(17) Liu, X.; Qi, C.; Bing, T.; Cheng, X.; Shangguan, D. Highly Selective Phthalocyanine−Thymine Conjugate Sensor for Hg^{2+} Based on Target Induced Aggregation. *Anal. Chem.* **2009**, *81*, 3699−3704.

(18) Volpati, D.; Alessio, P.; Zanfolim, A. A.; Storti, F. C.; Job, A. E.; Ferreira, M.; Riul, A.; Oliveira, O. N.; Constantino, C. J. L. Exploiting Distinct Molecular Architectures of Ultrathin Films Made with Iron Phthalocyanine for Sensing. *J. Phys. Chem. B* **2008**, *112*, 15275−15282.

(19) Peeters, K.; De Wael, K. D.; Bogaert, D.; Adriaens, A. The Electrochemical Detection of 4-Chlorophenol at Gold Electrodes Modified with Different Phthalocyanines. *Sens. Actuators, B* **2008**, *128*, 494−499.

(20) Liu, Y.; Dong, X.; Chen, P. Biological and Chemical Sensors Based on Graphene Materials. *Chem. Soc. Rev.* **2012**, *41*, 2283−2307.

(21) Casabianca, L. B.; Shaibat, M. A.; Cai, W. W.; Park, S.; Piner, R.; Ruoff, R. S.; Ishii, Y. NMR-Based Structural Modeling of Graphite Oxide Using Multidimensional ^{13}C Solid-State NMR and ab Initio Chemical Shift Calculations. *J. Am. Chem. Soc.* **2010**, *132*, 5672−5676.

(22) Dikin, D. A.; Stankovich, S.; Zimney, E. J.; Piner, R. D.; Dommett, G. H. B.; Evmenenko, G.; Nguyen, S. T.; Ruoff, R. S. Preparation and Characterization of Graphene Oxide Paper. *Nature* **2007**, *448*, 457−460.

(23) Mohanty, N.; Berry, V. Graphene-Based Single-Bacterium Resolution Biodevice and DNA Transistor: Interfacing Graphene Derivatives with Nanoscale and Microscale Biocomponents. *Nano Lett.* **2008**, *8*, 4469−4476.

(24) Wu, H.; Fan, S.; Jin, X.; Zhang, H.; Chen, H.; Dai, Z.; Zou, X. Construction of a Zinc Porphyrin−Fullerene-Derivative Based Non-enzymatic Electrochemical Sensor for Sensitive Sensing of Hydrogen Peroxide and Nitrite. *Anal. Chem.* **2014**, *86*, 6285−6290.

(25) Simon, J.; Bassoul, P. *Design of Molecular Materials: Supramolecular Engineering*; John Wiley & Sons: London, 2001; pp 196−296.

(26) Ulman, A. *An Introduction to Ultrthin Organic Films*; Academic Press: San Diego, CA, 1991.

(27) Jiang, J.; Ng, D. K. P. A Decade Journey in the Chemistry of Sandwich-Type Tetrapyrrolato−Rare Earth Complexes. *Acc. Chem. Res.* **2009**, *42*, 79−88.

(28) Jiang, J.; Bao, M.; Rintoul, L.; Arnold, D. P. Vibrational Spectroscopy of Phthalocyanine and Naphthalocyanine in Sandwich-Type (Na)Phthalocyaninato and Porphyrinato Rare Earth Complexes. *Coord. Chem. Rev.* **2006**, *250*, 424−448.

(29) Jiang, J.; Kasuga, K.; Arnold, D. P. In *Supramolecular Photosensitive and Electroactive Materials*; Nalwa, H. S., Ed.; New York, 2001; Chapter 2, pp113−210.

(30) Ng, D. K. P.; Jiang, J. Sandwich-Type Heteroleptic Phthalocyaninato and Porphyrinato Metal Complexes. *Chem. Soc. Rev.* **1997**, *26*, 433−442.

(31) Yoshimoto, S.; Sawaguchi, T.; Su, W.; Jiang, J.; Kobayashi, N. Superstructure Formation and Rearrangement in the Adlayer of a Rare-Earth-Metal Triple-Decker Sandwich Complex at the Electrochemical Interface. *Angew. Chem., Int. Ed.* **2007**, *46*, 1071−1074.

(32) Ye, T.; Takami, T.; Wang, R.; Jiang, J.; Weiss, P. S. Tuning Interactions between Ligands in Self-Assembled Double-Decker Phthalocyanine Arrays. *J. Am. Chem. Soc.* **2006**, *128*, 10984−10985.

(33) Lu, G.; Chen, Y.; Zhang, X.; Bao, M.; Bian, Y.; Li, X.; Jiang, J. Morphology Controlled Self-Assembled Nanostructures of Sandwich Mixed (Phthalocyaninato) (Porphyrinato) Europium Triple-Deckers. Effect of Hydrogen Bonding on Tuning the Intermolecular Interaction. *J. Am. Chem. Soc.* **2008**, *130*, 11623−11630.

(34) Bard, A. J.; Faulkner, L. R. *Electrochemical Methods-Fundamentals and Applications*; Wiley: New York, 1984.

(35) Tang, M. L.; Reichardt, A. D.; Wei, P.; Bao, Z. Correlating Carrier Type with Frontier Molecular Orbital Energy Levels in Organic Thin Film Transistors of Functionalized Acene Derivatives. *J. Am. Chem. Soc.* **2009**, *131*, 5264−5273.

(36) Li, H.; Gan, S.; Han, D.; Ma, W.; Cai, B.; Zhang, W.; Zhang, Q.; Niu, L. High Performance Pd Nanocrystals Supported on SnO_2-Decorated Graphene for Aromatic Nitro Compound Reduction. *J. Mater. Chem. A* **2014**, *2*, 3461−3467.

(37) Li, Y.; Zhang, P.; Ouyang, Z.; Zhang, M.; Lin, Z.; Li, J.; Su, Z.; Wei, G. Nanoscale Graphene Doped with Highly Dispersed Silver Nanoparticles: Quick Synthesis, Facile Fabrication of 3D Membrane-

DOI: 10.1021/acsami.6b08760
ACS Appl. Mater. Interfaces XXXX, XXX, XXX−XXX

Modified Electrode, and Super Performance for Electrochemical Sensing. *Adv. Funct. Mater.* **2016**, *26*, 2122−2134.
(38) Zhou, J.; Chen, M.; Xie, J.; Diao, G. Synergistically Enhanced Electrochemical Response of Host−Guest Recognition Based on Ternary Nanocomposites: Reduced Graphene Oxide-Amphiphilic Pillar[5]arene-Gold Nanoparticles. *ACS Appl. Mater. Interfaces* **2013**, *5*, 11218−11224.
(39) Gao, D.; Zhang, X.; Kong, X.; Chen, Y.; Jiang, J. (TFPP)Eu[$Pc(OPh)_8$]Eu[$Pc(OPh)_8$]/CuPc Two-Component Bilayer Heterojunction-Based Organic Transistors with High Ambipolar Performance. *ACS Appl. Mater. Interfaces* **2015**, *7*, 2486−2493.
(40) Mack, J.; Stillman, M. J.; Kobayashi, N. Application of MCD Spectroscopy to Porphyrinoids. *Coord. Chem. Rev.* **2007**, *251*, 429−453.
(41) Kasha, M.; Rawls, H. R.; Ashraf El-Bayoumi, M. A. The Exciton Model in Molecular Spectroscopy. *Pure Appl. Chem.* **1965**, *11*, 371−392.
(42) Cook, M. J.; Chambrier, I. In *Porphyrin Handbook*; Kadsh, K. M., Smith, K. M., Guilard, R., Eds.; Academic: San Diego, CA, 2003; Vol. *17*, pp 37−127.
(43) Zhang, X.; Chen, Y. A Sandwich Mixed (Phthalocyaninato) (Porphyrinato) Europium Triple-Decker: Balanced-Mobility, Ambipolar Organic Thin-Film Transistor. *Inorg. Chem. Commun.* **2014**, *39*, 79−82.
(44) Yoneyama, M.; Sugi, M.; Saito, M.; Ikegami, K.; Kuroda, S.; Iizima, S. Photoelectric Properties of Copper Phthalocyanine Langmuir-Blodgett Film. *Jpn. J. Appl. Phys.* **1986**, *25*, 961−966.
(45) Clark, B. J.; Frost, T.; Russell, M. A. *UV Spectroscopy: Techniques, Instrumentation, Data Handling*; Chapman & Hall: London, 1993; Vol. *4*.
(46) Chen, J.; Yan, X.; Meng, K.; Wang, S. Graphene Oxide Based Photoinduced Charge Transfer Label-Free Near-Infrared Fluorescent Biosensor for Dopamine. *Anal. Chem.* **2011**, *83*, 8787−8793.
(47) Bao, C.; Song, L.; Xing, W.; Yuan, B.; Wilkie, C. A.; Huang, J.; Guo, Y.; Hu, Y. Preparation of Graphene by Pressurized Oxidation and Multiplex Reduction and its Polymer Nanocomposites by Masterbatch-Based Melt Blending. *J. Mater. Chem.* **2012**, *22*, 6088−6096.
(48) Bao, C.; Guo, Y.; Song, L.; Hu, Y. Poly(Vinyl Alcohol) Nanocomposites Based on Graphene and Graphite Oxide: A Comparative Investigation of Property and Mechanism. *J. Mater. Chem.* **2011**, *21*, 13942−13950.
(49) Lu, G.; Kong, X.; Ma, P.; Wang, K.; Chen, Y.; Jiang, J. Amphiphilic (Phthalocyaninato) (Porphyrinato) Europium Triple-Decker Nanoribbons with Air-Stable Ambipolar OFET Performance. *ACS Appl. Mater. Interfaces* **2016**, *8*, 6174−6182.
(50) Lu, G.; Zhang, X.; Cai, X.; Jiang, J. Tuning the Morphology of Self-Assembled Nanostructures of Amphiphilic Tetra(P-Hydroxyphenyl) Porphyrins with Hydrogen Bonding and Metal−Ligand Coordination Bonding. *J. Mater. Chem.* **2009**, *19*, 2417−2424.
(51) Chen, Y.; Zhao, S.; Li, X.; Jiang, J. Tuning the Arrangement of Mono-Crown Ether-Substituted Phthalocyanines in Langmuir−Blodgett Films by the Length of Alkyl Chains and the Cation in Subphase. *J. Colloid Interface Sci.* **2005**, *289*, 200−205.
(52) Li, D.; Wang, H.; Kan, J.; Lu, W.; Chen, Y.; Jiang, J. H-Aggregation Mode in Triple-Decker Phthalocyaninato-Europium Semiconductors. Materials Design for High-Performance Air-Stable Ambipolar Organic Thin Film Transistors. *Org. Electron.* **2013**, *14*, 2582−2589.
(53) Rivnay, J.; Steyrleuthner, R.; Jimison, L. H.; Casadei, A.; Chen, Z.; Toney, M. F.; Facchetti, A.; Neher, D.; Salleo, A. Drastic Control of Texture in a High Performance n-Type Polymeric Semiconductor and Implications for Charge Transport. *Macromolecules* **2011**, *44*, 5246−5255.
(54) An, N.; Shi, Y.; Feng, J.; Li, D.; Gao, J.; Chen, Y.; Li, X. N-Channel Organic Thin-Film Transistors Based on a Soluble Cyclized Perylene Tetracarboxylic Diimide Dimer. *Org. Electron.* **2013**, *14*, 1197−1203.
(55) Usta, H.; Risko, C.; Wang, Z.; Huang, H.; Deliomeroglu, M. K.; Zhukhovitskiy, A.; Facchetti, A.; Marks, T. J. Design, Synthesis, and Characterization of Ladder-Type Molecules and Polymers. Air-Stable, Solution-Processable n-Channel and Ambipolar Semiconductors for Thin-Film Transistors via Experiment and Theory. *J. Am. Chem. Soc.* **2009**, *131*, 5586−5608.
(56) Lei, T.; Dou, J.; Ma, Z.; Liu, C.; Wang, J.; Pei, J. Chlorination as a Useful Method to Modulate Conjugated Polymers: Balanced and Ambient-Stable Ambipolar High-Performance Field-Effect Transistors and Inverters Based on Chlorinated Isoindigo Polymers. *Chem. Sci.* **2013**, *4*, 2447−2452.
(57) Chen, L.; Tang, Y.; Wang, K.; Liu, C.; Luo, S. Direct Electrodeposition of Reduced Graphene Oxide on Glassy Carbon Electrode and Its Electrochemical Application. *Electrochem. Commun.* **2011**, *13*, 133−137.
(58) Arrieta, A.; Rodrıguez-Mendez, M. L.; De Saja, J. A. Langmuir−Blodgett Film and Carbon Paste Electrodes Based on Phthalocyanines as Sensing Units for Taste. *Sens. Actuators, B* **2003**, *95*, 357−365.
(59) Alessio, P.; Pavinatto, F. J.; Oliveira, O. N., Jr.; De Saja Sa, J. A.; Constantino, C. J. L.; Rodrıguez-Mendez, M. L. Detection of Catechol Using Mixed Langmuir−Blodgett Films of A Phospholipid and Phthalocyanines as Voltammetric Sensors. *Analyst* **2010**, *135*, 2591−2599.
(60) Chaves, J. A. P.; Araujo, M. F. A.; Varela Júnior, J. de J. G.; Tanaka, A. A. Eletrocatálise Da Reação De Redução De Oxigênio Sobre Eletrodos De Grafite Modificados Com Ftalocianina Tetracarboxilada De Ferro. *Ecletica Quim.* **2003**, *28*, 9−20.
(61) Corio, P.; Rubim, J. C.; Aroca, R. Contribution of the Herzberg−Teller Mechanism to the Surface-Enhanced Raman Scattering of Iron Phthalocyanine Adsorbed on a Silver Electrode. *Langmuir* **1998**, *14*, 4162−4168.
(62) Maji, S. K.; Sreejith, S.; Mandal, A. K.; Ma, X.; Zhao, Y. Immobilizing Gold Nanoparticles in Mesoporous Silica Covered Reduced Graphene Oxide: A Hybrid Material for Cancer Cell Detection through Hydrogen Peroxide Sensing. *ACS Appl. Mater. Interfaces* **2014**, *6*, 13648−13656.
(63) de Oliveira Matos, I.; Alves, W. A. Electrochemical Determination of Dopamine Based on Self-Assembled Peptide Nanostructure. *ACS Appl. Mater. Interfaces* **2011**, *3*, 4437−4443.
(64) Zhang, P.; Zhao, X.; Zhang, X.; Lai, Y.; Wang, X.; Li, J.; Wei, G.; Su, Z. Electrospun Doping of Carbon Nanotubes and PlatinumNanoparticles into the β-Phase Polyvinylidene Difluoride Nanofibrous Membrane for Biosensor and Catalysis Applications. *ACS Appl. Mater. Interfaces* **2014**, *6*, 7563−7571.
(65) Saxberg, B. E. H.; Kowalski, R. Generalized Standard Addition Method. *Anal. Chem.* **1979**, *51*, 1031−1038.
(66) Kovtyukhova, N. I.; Ollivier, P. J.; Martin, B. R.; Mallouk, T. E.; Chizhik, S. A.; Buzaneva, E. V.; Gorchinskiy, A. D. Layer-by-Layer Assembly of Ultrathin Composite Films from Micron-Sized Graphite Oxide Sheets and Polycations. *Chem. Mater.* **1999**, *11*, 771−778.
(67) Li, H.; Gan, S.; Wang, H.; Han, D.; Niu, L. Intercorrelated Superhybrid of AgBr Supported on Graphitic-C_3N_4-Decorated Nitrogen-Doped Graphene: High Engineering Photocatalytic Activities for Water Purification and CO_2 Reduction. *Adv. Mater.* **2015**, *27*, 6906−6913.
(68) Bian, Y.; Jiang, J.; Tao, Y.; Choi, M. T. M.; Li, R.; Ng, A. C. H.; Zhu, P.; Pan, N.; Sun, X.; Arnold, D. P.; Zhou, Z.; Li, H.; Mak, T. C. W.; Ng, D. K. P. Tuning the Valence of the Cerium Center in (Na)phthalocyaninato and Porphyrinato Cerium Double-Deckers by Changing the Nature of the Tetrapyrrole Ligands. *J. Am. Chem. Soc.* **2003**, *125*, 12257−12267.
(69) Kim, H.; Jang, Y. R.; Yoo, J.; Seo, Y.; Kim, K.; Lee, J.; Park, S.; Kim, C.; Koo, J. Morphology Control of Surfactant-Assisted Graphene Oxide Films at the Liquid−Gas Interface. *Langmuir* **2014**, *30*, 2170−2177.

DOI: 10.1021/acsami.6b08760
ACS Appl. Mater. Interfaces XXXX, XXX, XXX−XXX